



# Simulation of a 100-MW solar-powered thermo-chemical air separation system combined with an oxy-fuel power plant for bio-energy with carbon capture and storage (BECCS)

Clemens F. Patzschke<sup>1</sup> · Husain Bahzad<sup>1</sup> · Matthew E. Boot-Handford<sup>1</sup> · Paul S. Fennell<sup>1</sup>

Received: 5 December 2018 / Accepted: 27 June 2019 / Published online: 10 August 2019  
© The Author(s) 2019

## Abstract

The combination of concentrated solar power–chemical looping air separation (CSP-CLAS) with an oxy-fuel combustion process for carbon dioxide (CO<sub>2</sub>) capture is a novel system to generate electricity from solar power and biomass while being able to store solar power efficiently. In this study, the computer program Advanced System for Process Engineering Plus (ASPEN Plus) was used to develop models to assess the process performance of such a process with manganese (Mn)-based oxygen carriers on alumina (Al<sub>2</sub>O<sub>3</sub>) support for a location in the region of Seville in Spain, using real solar beam irradiance and electricity demand data. It was shown that the utilisation of olive tree prunings (*Olea europaea*) as the fuel—an agricultural residue produced locally—results in negative CO<sub>2</sub> emissions (a net removal of CO<sub>2</sub> from the atmosphere). Furthermore, it was found that the process with an annual average electricity output of 18 MW would utilise 2.43% of Andalusia’s olive tree prunings, thereby capturing 260.5 k-tonnes of CO<sub>2</sub>, annually. Drawbacks of the system are its relatively high complexity, a significant energy penalty in the CLAS process associated with the steam requirements for the loop-seal fluidisation, and the gas storage requirements. Nevertheless, the utilisation of agricultural residues is highly promising, and given the large quantities produced globally (~4 billion tonnes/year), it is suggested that other novel processes tailored to these fuels should be investigated, under consideration of a future price on CO<sub>2</sub> emissions, integration potential with a likely electricity grid system, and based on the local conditions and real data.

---

✉ Paul S. Fennell  
p.fennell@imperial.ac.uk

<sup>1</sup> Department of Chemical Engineering, Imperial College London, South Kensington Campus, London SW7 2AZ, UK

**Keywords** Chemical looping air separation (CLAS) · Mn oxygen carrier · BECCS · Energy storage · Concentrated solar power (CSP) · Negative CO<sub>2</sub> emissions · Climate change mitigation · Chemical looping · CLOU · Oxygen uncoupling · Bio energy with CO<sub>2</sub> capture · CO<sub>2</sub> capture · Olive tree pruning · Olive grove

## 1 Introduction

The primary driver of climate change is anthropogenic emissions of carbon dioxide (CO<sub>2</sub>) (IPCC 2005). A high share of this is coming from the burning of fossil fuels for transport, energy production and industrial processes (IPCC 2005). Oxy-fuel combustion is a novel combustion process, which is based on the substitution of air with oxygen (O<sub>2</sub>)-enriched recycled flue gas during combustion. This results in the production of a CO<sub>2</sub>-rich stream. After removal of steam (H<sub>2</sub>O) and impurities, the CO<sub>2</sub> stream can be compressed and permanently sequestered in geological formations. The production of O<sub>2</sub> is conventionally done via cryogenic distillation, which results in a relatively high energy penalty (~0.4 kWh/m<sup>3</sup><sub>n</sub>) for air separation (Zhou et al. 2015). Recently, chemical looping air separation (CLAS) has been proposed for air separation (Moghtaderi 2010). To achieve the same combustion characteristics, a higher O<sub>2</sub> volume fraction (here assumed to be 27 vol%) is required during oxy-fuel combustion than during combustion in air (Riaza et al. 2012). Tagliaferri et al. (Tagliaferri et al. 2018) carried out a life cycle assessment of various systems for electricity production and reported that the CLAS + oxy-fuel process had the lowest (and only negative) global warming potential in comparison with the other studied conventional and novel fossil fuel and renewable electricity generation technologies. In this study, the enthalpy required for the O<sub>2</sub> uncoupling is provided by concentrated solar power, and storage of O<sub>2</sub>+CO<sub>2</sub> and CO<sub>2</sub> enables operation of the CLAS process and the oxy-fuel process at different times of the day. The process is illustrated in Fig. 1(a). This bio-energy with carbon capture and storage (BECCS) process can result in a net transfer of carbon from the atmosphere to the geosphere (negative CO<sub>2</sub> emissions), as illustrated in Fig. 1(b).

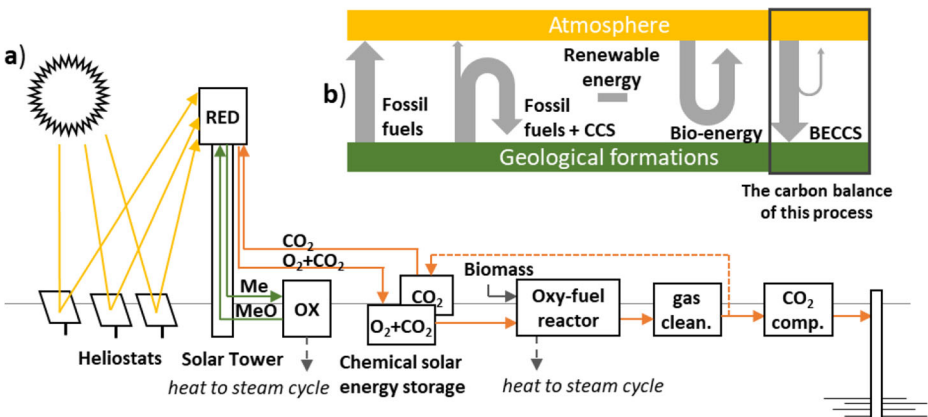


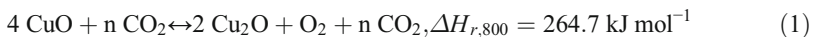
**Fig. 1** (a) Schematic diagram of the solar-powered CLAS process combined with an oxy-fuel process for BECCS and (b) carbon balances of power generation processes with a highlighted balance for BECCS adapted from Karlsson and Byström (2011)

The simulated plant is assumed to be located in the region of Seville in Spain, where other prototypes of concentrated solar power (CSP) plants are currently tested (NREL 2018), and for which detailed sun irradiance data is available (Blair et al. 2018). Seville is located in Andalusia. The criterion for the selection of biomass for combustion in the BECCS plant was that it had to be produced in Andalusia to minimise emissions for transportation of the fuel. Figure 2, below, illustrates the cumulated energy contained in different types of biomass produced in Andalusia.

The biomass type with the largest energy potential in Fig. 2 is olive grove—the pruning of olive trees. It is an agricultural residue that is currently either illegally burned or left on the ground to decay (García-Maraver et al. 2012). In both cases, the contained carbon is released as CO<sub>2</sub> into the atmosphere. In Andalusia, about four million tons of olive tree pruning are produced annually. Owing to the availability and quantity of this type of biomass, olive tree prunings were selected as the fuel for the BECCS plant in this study.

Next, the oxygen storage material was selected. Only some transition metal oxides systems, such as those containing cobalt (Co) (Li et al. 2008; Moghtaderi 2010; Shah et al. 2012), copper (Cu) (Moghtaderi 2010; Shah et al. 2012; Song et al. 2014) or manganese (Mn) (Moghtaderi 2010, Shah et al. 2012) are capable of releasing gaseous O<sub>2</sub> in CO<sub>2</sub> at conditions that are relevant for the CLAS process. Co-based oxygen carriers are toxic and irreversibly react with oxides of sulphur (S) in the recycled flue gases to produce CoSO<sub>4</sub> within the temperature range of a CLAS process (800–900 °C). As a consequence, Co-based oxygen carriers were removed from consideration (Shah et al. 2013).

The system CuO/Cu<sub>2</sub>O, which reacts according to



has the highest theoretical oxygen carrying capacity (mass of O<sub>2</sub> available for uncoupling/mass of fully oxidised oxygen carrier) of the three transition metals with O<sub>2</sub> release functionality of 10.1 wt%. However, the phase equilibrium temperature within an atmosphere of 27 vol% O<sub>2</sub> is 1026 °C, which means that even higher temperatures are needed to release O<sub>2</sub> with sufficiently high rates. These temperatures are approaching

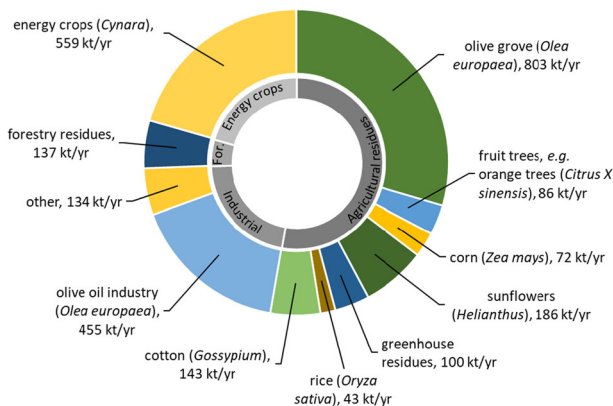


**Fig. 2** Biomass potential in Andalusia in kilotonne oil equivalent (ktOE) per annum, excluding municipal sewage sludge, mud and animal waste. The data is taken from García-Maraver et al. (2012)

upper metallurgical limits for Cu-based oxygen carriers and beyond those possible with current state-of-the-art CSP technology. A further disadvantage of the copper oxides is their inferior mechanical properties, making them prone to agglomeration and attrition (Cho et al. 2004).

$Mn_2O_3/Mn_3O_4$  reacts according to



The  $O_2$  release capacity of  $Mn_2O_3/Mn_3O_4$  (3.4 wt%) is lower than that of  $CuO/Cu_2O$ , but the position of the phase equilibrium temperature in 27 vol%  $O_2$  is lower at 916 °C. To have sufficiently high kinetics, the reducer would operate at a temperature of around 950 °C, which is within the range at which current CSP systems can provide heat. As such, Mn-based materials are the only feasible single-metal oxide oxygen storage materials suitable for CSP-CLAS with current state-of-the-art CSP technology and reactor vessel materials. The combination of a CSP-CLAS system with the combustion of biomass in oxy-fuel mode is the subject of this study. This combined process would allow to achieve negative  $CO_2$  emissions as well as to storage solar energy in the form of  $O_2$ -enriched  $CO_2$  for the operation of the BECCS plant at during the night-time.

## 2 Description and modelling of the process

The process consists of four subsystems: (i) the CSP-CLAS system, (ii) an  $O_2+CO_2$  storage system, (iii) the oxy-fuel combustion system and (iv) the steam cycle. The flow sheet of the model developed in the chemical engineering modelling program, ASPEN Plus, of this process is shown in Fig. 3, below.

The considerations leading to the design of this process are described in detail in the sections below.

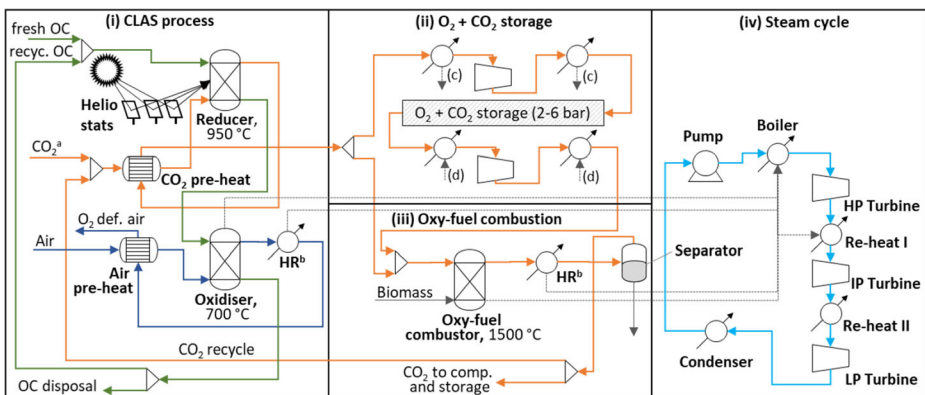


**Fig. 3** Flow sheet of the process of this study. The streams are coloured to indicate flows of oxygen carriers (green),  $CO_2$  and  $O_2+CO_2$  (orange), air and  $O_2$ -deficient air (dark blue) and steam (light blue). (a)  $CO_2$  stream from gas storage during operation of the CLAS process when the BECCS plant is not producing sufficient  $CO_2$ . (b) HR abbreviates ‘heat recovery’. (c) Heat stream from  $O_2+CO_2$  compression is used to preheat air. (d) Heat stream into  $O_2+CO_2$  expansion is provided from oxy-fuel heat recovery

## 2.1 Concentrated solar power

The heat required for the endothermic reaction of the  $O_2$  uncoupling is provided by concentrated solar power. A suitable design for the collectors is a heliostat field, which consists of an array of planar mirrors (Barlev et al. 2011). The mirrors are reflecting the incident sunlight focused on the receiver, which is located on the top of a tower in the centre of the array (Barlev et al. 2011). The solar power heat flow,  $\dot{Q}_{CSP}$ , was calculated by

$$\dot{Q}_{CSP} = R_{BI} \cdot A_{HS} \cdot \eta_{HS+R}, \quad (3)$$

where  $R_{BI}$  is the area specific solar beam irradiance,  $A_{HS}$  the area of the panels of the heliostats and  $\eta_{HS+R}$  the combined efficiency of the heliostats and the receiver. For  $\eta_{HS+R}$ , a value of 0.49 was assumed (Zhang et al. 2013). The data for the beam irradiance for Seville in Spain was taken from the System Advisor Model (SAM) (Blair et al. 2018)—a performance calculator and database developed by the US D.o.E.'s National Renewable Energy Laboratory (NREL). The hourly beam irradiance data averaged for selected months is shown in Fig. 4, below.

## 2.2 The chemical looping air separation system

In this study, the reducer is defined as the reactor in which the oxygen carrier releases gaseous  $O_2$ , while the oxidation states of the oxygen carriers' active material are reduced. The reactor is assumed to operate at atmospheric pressure and was modelled in ASPEN Plus as a RGIBBS reactor—an equilibrium reactor. The operating temperature of the reactor was set to 916 °C to obtain an  $O_2$  outlet concentration of 27 vol%. The oxidiser also operates at atmospheric pressure and was modelled as an RGIBBS reactor, too. In reality, both reactors would likely be fluidised bed reactors with a solid-recycle. The outlet concentration of the oxidiser was assumed to be 8 vol%, which corresponds to an operating temperature of the RGIBBS reactor of 700 °C. Significantly lower  $O_2$  volume fractions at the outlet would result in slow reaction

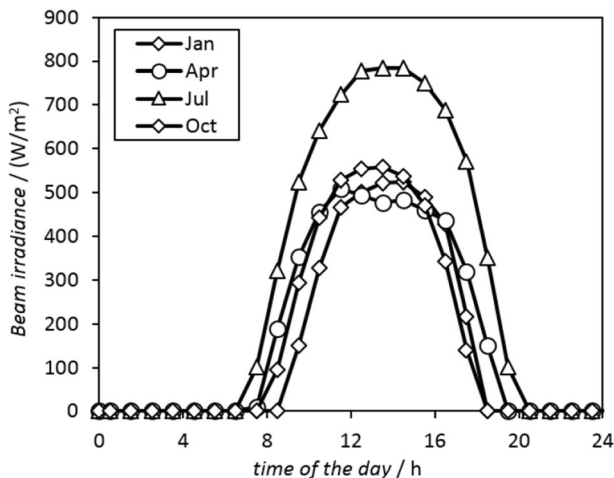


**Fig. 4** Solar beam irradiance data from the SAM tool for the region Seville, Spain. The hourly solar energy input into the CLAS system of this study was calculated using the solar beam irradiance data and Eq. (3)

**Table 1** Proximate analysis, calorific value and ultimate analysis of olive tree pruning, which is used as the fuel in this study (Vamvuka et al. 2014)

Proximate analysis (wt%)	Wet	Dry	Ultimate analysis (wt%)	Dry
Fixed carbon	19.0	21.3	Carbon	48.5
Volatile matter	69.4	77.9	Hydrogen	5.3
Ash	0.7	0.8	Oxygen	44.7
Moisture	11.0 <sup>a</sup>	0.0	Nitrogen	0.7
			Sulphur	0.0
<b>Higher heating value (HHV)</b>			Ash	0.8
HHV on dry basis:		19.1 MJ/kg	Moisture	0.0

The moisture content of ‘wet’ olive tree pruning was taken from García-Maraver et al. (2012)

rates, resulting in a larger and more capital intense oxidiser (Lyngfelt et al. 2001). A constant temperature in the oxidiser is maintained by transferring excess heat to the steam cycle. A further heat recovery unit downstream of the oxidiser utilises some of the enthalpy contained in the exhaust gas stream, thereby cooling it down to 600 °C. This recovered heat is also transferred to the steam cycle. The exhaust gas leaving this heat recovery unit and the gas stream leaving the reducer are used to preheat the cold air stream (to about 600 °C) and the cold O<sub>2</sub>+CO<sub>2</sub> stream (to about 900 °C), respectively. Loop-seals—a pneumatical sealing assembly that allows the oxygen carriers entering the reactor while preventing gas leakage from the reactor—are used at the oxygen carrier inlet of the oxidiser and the reducer. These seals are assumed to be fluidised with process steam. Marx et al. (2013) reported for pilot plant test in a 10 MW<sub>th</sub> unit steam requirements for the fluidisation of the loop-seal to the fuel reactor and to the air reactor of 178.2 kg h<sup>-1</sup> and 169.9 kg h<sup>-1</sup>, respectively. It was assumed that through careful design of the loop-seals, the steam requirements in an industrial-scale process can be reduced by 50% (Zerobin et al. 2016), which corresponds to a steam-to-oxygen carrier mass ratio of about 0.0257 for both loop-seals. To estimate the steam requirements for the CLAS process of this study, the value was linearly extrapolated to match the oxygen carrier circulation rate.

### 2.3 Oxy-fuel combustion of biomass

Olive tree prunings are taken as the solid fuel for the oxy-fuel combustion. The simulation of the solid fuel was carried out using the non-conventional solids package in ASPEN Plus, with the solid fuel specifications as summarised in Table 1, below.

The biomass drying and biomass combustion were modelled according to the ASPEN Plus’s standard procedure for the combustion of non-conventional solids (AspenTech 2013). This involved a RSTOIC reactor (a stoichiometric reactor in which the extent or conversion of the reaction is specified) for the biomass drying, in which the moisture content was reduced

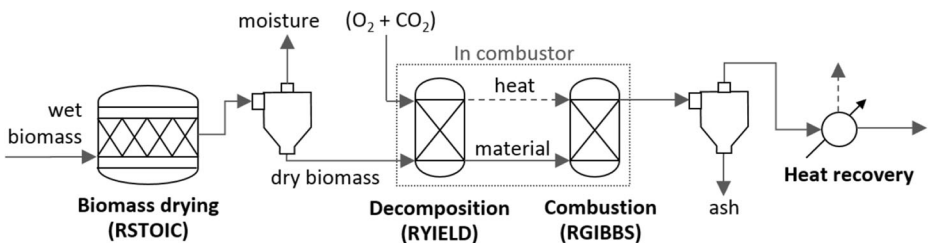


**Fig. 5** The reactor configuration in ASPEN Plus for the simulation of the drying and combustion of biomass

from 11.0 wt% to zero, as well as a RYIELD reactor (a reactor for which the yield of products is specified) and a RGIBBS reactor for the decomposition and the combustion, respectively. Those were followed by a separator (SSPLIT), to separate the ash and the combustion products. The heat of the combustion products was transferred to the steam cycle. The process is illustrated in Fig. 5, below.

In a typical simulation, the composition of the flue gas leaving the oxy-fuel combustor was  $CO_2 = 80.5 \text{ vol\%}$ ,  $H_2O = 15.1 \text{ vol\%}$ ,  $O_2 = 0.9 \text{ vol\%}$ ,  $N_2 = 0.2 \text{ vol\%}$ ,  $H_2 = 0.1 \text{ vol\%}$ .

### 2.4 Steam cycle, electricity generation and heat integration

The heat generated in the oxy-fuel combustor is utilised to raise steam to run a low-pressure (LP), an intermediate-pressure (IP), and a high-pressure (HP) steam turbine (ST), via a heat recovery steam generator (HRSG). The operating conditions of the parts of the steam cycle are summarised in Table 2, below.

The fuel used in this study is olive tree prunings, and the higher heating value (HHV) is assumed to be 19.1 MJ/kg (c.f. Table 1), as reported in Vamvuka et al. (2014). The net plant efficiency of the combined process,  $\eta_{\text{plant}}$ , is calculated by the equation proposed by Porrazzo et al. (2016):

$$\eta_{\text{plant}} = \frac{W_{\text{total}}}{\dot{Q}_{\text{biomass}} + \dot{Q}_{\text{solar}}} = \frac{W_{\text{turbines}} - W_{\text{compressors}} - W_{\text{pumps}}}{m_{\text{biomass}} \cdot HHV + A_{HS} \cdot R_{IB}} \tag{4}$$

where  $\dot{Q}_{\text{biomass}}$  is the heat released during the combustion of biomass, which is equal to the product of its mass flow rate,  $m_{\text{biomass}}$ , and its heating value,  $HHV$ .  $\dot{Q}_{\text{solar}}$  is the heat of incoming solar radiation, which in turn was calculated by Eq. (3). Therefore,  $\eta_{\text{plant}}$  refers to the total energy added to the system, which is the sum of the energy added by the two different types of primary energy carriers, viz. solar power and biomass.

$W_{\text{total}}$  is the total work available to run the electrical generators and  $W_{\text{turbines}}$ ,  $W_{\text{compressors}}$ , and  $W_{\text{pumps}}$  are the work of the turbines, compressors and pumps, respectively. The electrical power output was estimated by

$$P_{\text{elec.}} \approx \frac{W_{\text{turbines}} - W_{\text{compressors}} - W_{\text{pumps}}}{t} \tag{5}$$

where  $P_{\text{elec.}}$  is the electrical power output and  $t$  is time. The objective function was for  $P_{\text{elec.}}$  to be proportional to the hourly electricity demand of Spain at any given hour. The demand data

**Table 2** Operational parameter for the steady-state operation of the CSP-CLAS+oxy-fuel system

Stream	Inlet temperature (°C)	Outlet temperature (°C)	Pressure (bar)
HP steam from HRSG	30	613	260
HP steam to HP ST	613	515	150
IP steam to IP reheat	515	613	150
IP steam to IP ST	613	480	150
LP steam to LP reheat	480	613	70
LP steam to LP ST	613	33	70
Cooling water to condenser	30	30	0.043
Condensate return to HRSG	30	613	260

averaged for every calendar month of the year 2015 was taken from *The European Network of Transmission System Operators for Electricity* (ENTSOE) and is shown in Fig. 6, below (ENTSOE 2018).

## 2.5 Sizing of the CSP-CLAS and the oxy-fuel system

The CSP-CLAS and the oxy-fuel systems depend on each other, since the CSP-CLAS system produces the  $O_2+CO_2$ , which is consumed by the oxy-fuel system. Since the CLAS system operates predominantly during the day and the oxy-fuel system predominantly during the night, significant quantities of  $O_2+CO_2$  and  $CO_2$  need to be stored. The two boundary conditions to size the two systems were the following: (i) the input of thermal energy into the reducer of the CLAS system has to be equal to the hourly varying solar power calculated by Eq. (3) using the solar beam irradiance data for the region Seville, Spain, and (ii) the electricity output has to vary proportionally to Spain's hourly electricity demand (data from ENTSOE (2018) for the year 2015 was used). Before this dynamic simulation was conducted, a steady-state model with a 100-MW solar power input (at the receiver) was developed. In this steady-state simulation, the  $O_2+CO_2$  mixture produced in the CSP-CLAS system was directly used for the oxy-fuel combustion of the olive tree prunings (without intermediate gas storage). For the dynamic simulation, the flow rates of oxygen carrier and gaseous fuel as well as the split ratios that determined the amounts of 'gas stored' and 'gas directly utilised' were adjusted to produce variants of the system, with sun power input and electricity power output at any given hour of the day corresponding to the solar power input and electricity demand, respectively. Then, a third boundary condition was introduced, specifying that at the end of the day, the amount of  $O_2+CO_2$  stored has to equal the amount of gas stored at the beginning of the day. This boundary condition was applied by calculating the change of stored  $O_2+CO_2$  over 24 h. A negative balance, which means more  $O_2+CO_2$  was consumed over the course of the

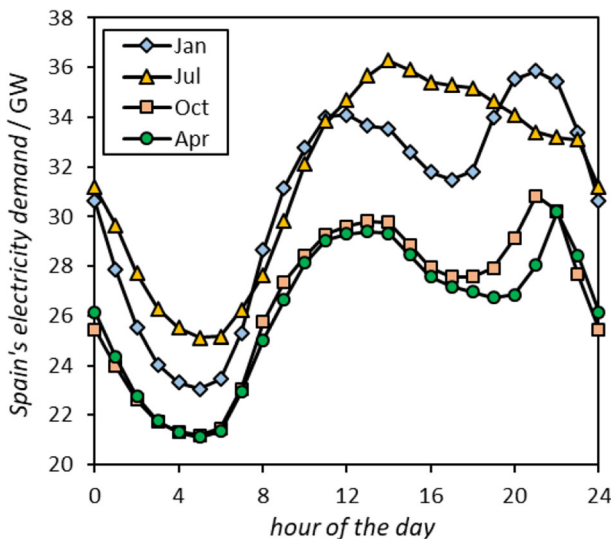


**Fig. 6** Spain's hourly electricity demand averaged for selected months. The objective function of the optimisation of this study was to produce electricity proportional to this energy demand. The data is taken from the European Network of Transmission System Operators for Electricity (ENTSOE 2018)



day than produced, implied that the BECCS plant combusts too much biomass and thus, the mass flow rate of biomass was reduced. A positive balance, in turn, meant that not all of the available  $O_2+CO_2$  was utilised, and the  $O_2+CO_2$  and biomass flow rate was thus increased. After adjusting the size of the BECCS plant, the performance of the plant was calculated for every hour of the day. This iteration was repeated until the amount of  $O_2+CO_2$  stored at the beginning of the day and the end of the day was the same. This iteration procedure was then repeated for the different cases (c.f. Fig. 6) as well as for the different months (c.f. Fig. 8). For the latter, solar radiation and electricity demand data for January, April, July and October were used.

### 3 Results and discussion

#### 3.1 Synergetic operation of both processes in steady-state

The results of the steady-state simulation are reported in Table 3, below.

Using Eq. (4), a net plant efficiency during steady-state of 26.3% was calculated. However, care has to be taken when comparing this value with calculated efficiencies of other thermal power plants, since here two types of energy carriers are used (solar power and biomass). When only operating the BECCS plant and the CSP-CLAS plant with the steam cycle, the steady-state net plant efficiency is 37.0% and 17.8%, respectively.

#### 3.2 Synergetic operation of both processes in dynamic mode

In dynamic operation and with a minimum load factor of the BECCS plant equal to zero, the two systems operate mostly separately—the BECCS system predominantly at night and the CSP-CLAS system during the hours of sunshine. Only a few hours of simultaneous operations occur during the mornings and evenings. This restricts the heat integration between the BECCS system and CSP-CLAS system. A further drawback of the independent operation is the energy penalty associated with gas storage. Firstly, the  $O_2$ -enriched  $CO_2$  is sent to storage at 80 °C, while is withdrawn from the storage at 20 °C. The energy of the difference in temperatures is assumed to be dissipated into the ground and hence lost from the system. Secondly, adiabatic and mechanical isentropic inefficiencies during compression of the  $O_2+CO_2$  to 2–6 bar and expansion back to atmospheric pressure result in further losses of energy.

**Table 3** Parameter and results of the steady-state simulation of the CSP-CLAS + oxy-fuel process

Parameters of the reducer		Parameters of oxy-fuel combustion	
Solar power to reducer	100 MW	Biomass feeding rate	24,907 kg/h
Mass flow rate of $CO_2$ (inlet)	113,845 kg/h	<b>Parameters of the steam cycle</b>	
Operating temperature	916 °C	$H_2O$ mass flow rate	58,392 kg/h
$O_2$ concentration at outlet	27 vol%	Power generated in LPT	20.9 MW
Flow rate of the $O_2+CO_2$	144,460 kg/h	Power generated in HPT	3.7 MW
Loop-seals fluidisation steam req.	2044 kg/h	Power generated in IPT	2.6 MW
<b>Parameters of the air reactor</b>		Power consumed by pumps	0.8 MW
Operating temperature	750 °C	Net power generated	26.3 MW
Oxygen carrier circulation rate	906 t/h	Net thermal efficiency	26.3%

Counterintuitively, the electricity-weighted net plant efficiency during dynamic operation is slightly higher than during steady-steady operation. This is because the BECCS plant runs for more hours per day and produces more energy than the CSP-CLAS system, and this inflates the calculated value.

The dynamic simulation of the process was carried out using the solar energy and electricity demand data of the month of July with different assumptions: In *case A*, the minimum load factor of the BECCS plant ( $LF_{\min}$ ) was set to zero, while in *case B*, *case C* and *case D*, the value of  $LF_{\min}$  is 21%. Ideally, the BECCS plant would shut off during the day when the CSP-CLAS system produces sufficient energy to meet the electricity demand and operate only when the CSP-CLAS system does not produce (sufficient) electricity. However, solid fuel power plants do typically not offer this flexibility, amongst others, since this would cause excessive erosion of the bearings and deterioration of the reactor materials due to the large temperature changes. The value of  $LF_{\min} = 21\%$ , which is used in *case B*, *case C* and *case D*, is a more realistic assumption.

Furthermore, in *case A* and *case B*, it is assumed that the active phase of the oxygen carriers, i.e.  $Mn_2O_3/Mn_3O_4$ , is unsupported. This is ideal from a thermodynamic standpoint, since the addition of a supporting material would result in a higher solid circulation rate. More material per unit of time would need to be heated in the reducer and subsequently cooled in the oxidiser. This effectively increases the transport of heat from the reducer to the oxidiser, which reduces the enthalpy that is available in the reducer for the endothermic  $O_2$  uncoupling, and thus in turn reduces the rate of  $O_2$  production in the CLAS process. During continuous redox-cycling unsupported Mn oxygen carriers would probably agglomerate. To prevent this, the  $Mn_2O_3$  is supported on 30 wt%  $Al_2O_3$  and 60 wt%  $Al_2O_3$  in *case C* and *case D*, respectively. The results of the four cases are shown in Fig. 7, below.

In Fig. 7(a), it can be seen that a process that operates with a  $LF_{\min}$  of zero and utilises unsupported  $Mn_2O_3$  oxygen carriers is able to produce 0.10% of Spain's electricity while following the hourly variations of Spain's electricity demand. When setting the  $LF_{\min}$  to 0.21% (Fig. 7(b)), it is no longer possible to produce an electricity supply that is proportional to the demand: during mid-day the supply of power from the CLAS process and the BECCS plant result in excess electricity (5.3% of the daily electricity production). Furthermore, only 0.09% of Spain's electricity demand can be supplied.

Supporting the active metal oxide on 30 wt%  $Al_2O_3$  (Fig. 7(c)) and 60 wt%  $Al_2O_3$  (Fig. 7(d)) decreases the energy storage potential further, so that 0.08% and 0.05% of Spain's electricity demand are supplied, while producing around mid-day excess electricity that corresponds to 14.1% and 36.0% of the daily electricity production, respectively.

The reduction of the electricity production with increasing supporting material mass fraction,  $\alpha_{\text{support}}$ , is predominantly owing to the reduction of the  $O_2$  production rate. The additional material increases the heat transfer between the reducer and the oxidiser, which reduces the enthalpy available for air separation. Additionally, more supporting material (and thus a higher oxygen carrier circulation rate) requires more steam for the loop-seal fluidisation. This steam is withdrawn upstream of the low-pressure turbine and thus effectively reduces the power available for electricity generation. The reduction of  $O_2$  production and electricity production with an increase in support material mass fraction is illustrated in Fig. 8 (a and b), respectively.

The assumptions of *case C* were deemed to be most realistic and were thus used to calculate the performance of the system over the course of a year. The maximum thermal power output of the BECCS plant for *case C* in July (Fig. 7(c)) was 58.7 MW. Assuming that this

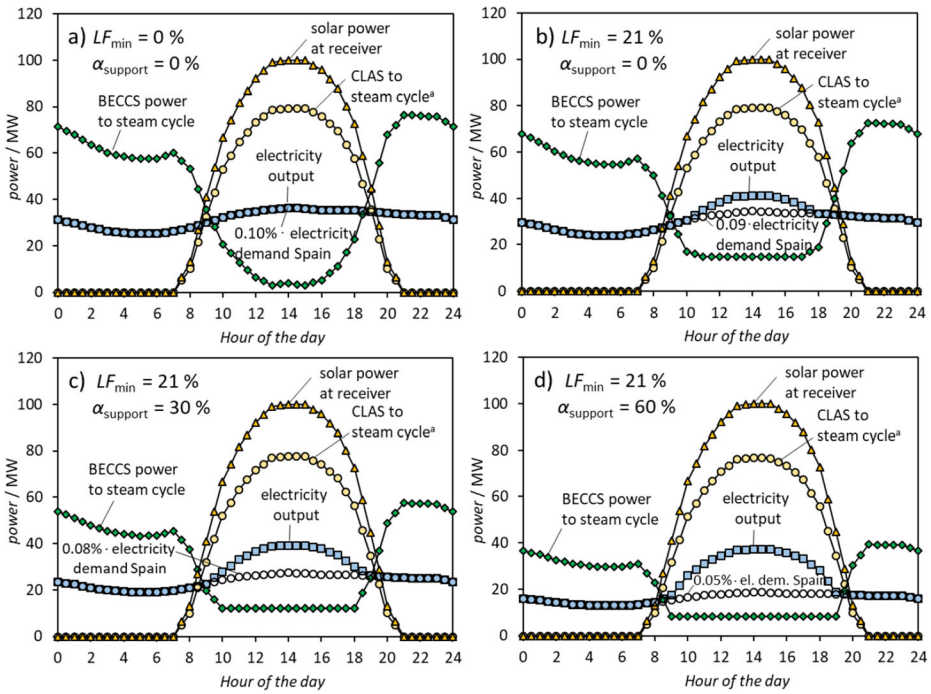


**Fig. 7** Power inputs and outputs of the subsystems and electricity demand over the course of the day, based on solar beam irradiance data and electricity demand data for the month of July with varying assumptions: (a) no minimum load factor of the BECCS plant,  $LF_{min}$ , and (b, c, d)  $LF_{min} = 21\% \sim 12.3$  MW; (a, b) unsupported  $Mn_2O_3$  oxygen carriers, (c)  $Mn_2O_3$  supported on 30 wt%  $Al_2O_3$ , and (d)  $Mn_2O_3$  supported on 60 wt%  $Al_2O_3$

corresponds to a load factor of 100%, the minimum load factor of 21% in this case corresponds to 12.3 MW. This power output was defined as the minimum power output of the BECCS plant for any given time and month of the year. Using the iteration procedure described in Section 2.5, the performance of the process was simulated for the different times of the year. The results are summarised in Table 4 below.

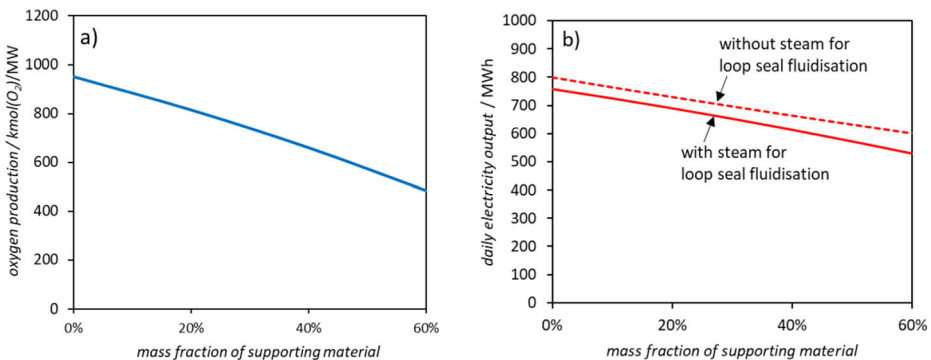


**Fig. 8** Plots of (a) the oxygen production per MW heat added to the reducer and (b) the daily electricity output of the plant as a function of supporting material mass fraction. For (b), the solar power and electricity demand data for the month of July was taken, and a minimum load factor of the BECCS plant of 22% was assumed

**Table 4** Power input and output of the subsystems (solar CLAS and BECCS) in MW at selected times of the day

Time	January					April					July					Oct				
	SP <sub>in</sub> <sup>a</sup>	CLAS <sup>b</sup>	BECCS <sup>c</sup>	Elec.	SP <sub>in</sub> <sup>a</sup>	CLAS <sup>b</sup>	BECCS <sup>c</sup>	Elec.	SP <sub>in</sub> <sup>a</sup>	CLAS <sup>b</sup>	BECCS <sup>c</sup>	Elec.	SP <sub>in</sub> <sup>a</sup>	CLAS <sup>b</sup>	BECCS <sup>c</sup>	Elec.	SP <sub>in</sub> <sup>a</sup>	CLAS <sup>b</sup>	BECCS <sup>c</sup>	Elec.
00:00	–	–	20	9	–	–	28	12	–	–	54	23	–	–	–	23	–	–	–	10
02:00	–	–	17	7	–	–	25	11	–	–	48	21	–	–	–	20	–	–	–	9
04:00	–	–	16	7	–	–	23	10	–	–	44	19	–	–	–	19	–	–	–	8
06:00	–	–	16	7	–	–	23	10	–	–	43	19	–	–	–	19	–	–	–	8
08:00	–	–	19	8	1	1	26	12	13	10	38	21	–	–	–	23	–	–	–	10
10:00	19	15	12	12	45	35	12	21	67	52	12	28	37	29	12	12	37	29	12	18
12:00	59	46	12	25	65	50	12	27	92	72	12	37	67	52	12	28	67	52	12	28
14:00	66	52	12	28	61	47	12	26	100	78	12	39	71	55	12	29	71	55	12	29
16:00	62	49	12	26	59	46	12	25	96	74	12	38	60	47	12	26	60	47	12	26
18:00	28	22	12	15	41	32	12	19	73	57	12	30	18	14	12	11	18	14	12	11
20:00	–	–	24	10	–	–	29	13	13	10	49	26	–	–	–	26	–	–	–	11
22:00	–	–	24	10	–	–	33	14	–	–	57	25	–	–	–	27	–	–	–	12

<sup>a</sup> Solar power heat flow into reducer in MW; <sup>b</sup> enthalpy from oxidiser and its downstream secondary heat recovery unit transferred to the steam cycle minus enthalpy requirement for steam utilised for loop-seal fluidisation; <sup>c</sup> enthalpy from BECCS process transferred to steam cycle

The results from Table 4 (together with further results of the simulation) are illustrated in Fig. 9, below.

In Table 4 and Fig. 9, it can be seen that the daily electricity production of the system varies significantly with the seasons. While in January, 331 MWh (Fig. 9(a)) is produced on an average day, the average daily electricity production for April, July and October is 397 MWh (Fig. 9(b)), 621 MWh (Fig. 9(c)) and 362 MWh (Fig. 9(d)), respectively. The lower electricity production in the colder months is mainly caused by less solar radiation. On the one hand, this results in less power transferred from the CLAS process to the steam cycle, and on the other hand, a lower  $O_2$  production rate, which in turn results in less  $O_2+CO_2$  being available for biomass combustion.

A reduced net plant efficiency and lower load factors of the BECCS are also caused by the lower solar radiation in the colder months. The monthly and annual average efficiencies (calculated for every hour using Eq. (7) and weighing the hourly values by the hourly electricity output) and the load factor of the BECCS process (calculated by dividing the actual daily power output by the maximum daily power output ( $57.8 \text{ MW} \times 24 \text{ h}$ )) are reported in Table 5, below.

The size of the array of heliostats can be determined from Eq. (3), which relates the solar beam irradiance and the solar power produced. When solving this equation for the area of the solar reflectors,  $A_{HS}$ , it results in a value of  $237,200 \text{ m}^2$ . This area is about three times larger than the area of the reflectors which power the nominal 11-MW<sub>el</sub> *Planta Solar 10* concentrated solar power plant ( $74,880 \text{ m}^2$ ) in Seville (NREL 2018).

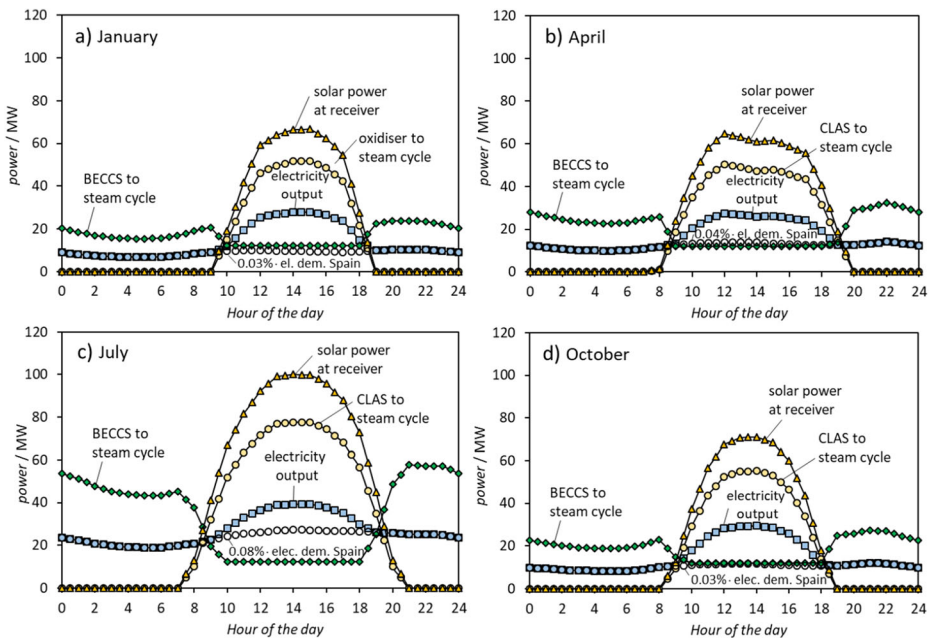


**Fig. 9** Power inputs and outputs of the subsystems and electricity demand over the course of the day with the assumptions of ‘case c’ (c.f. Fig. 6(c)): a minimum load factor of the BECCS plant,  $LF_{\min}$ , of 21%~12.3 MW and oxygen carriers containing  $Mn_2O_3$  and 30 wt%  $Al_2O_3$  for different months of the year: (a) January, (b) April, (c) July, and (d) October

**Table 5** Calculated thermal efficiencies and load factor of the CLAS + oxy-fuel

Case or month	Assumptions	Net plant efficiency <sup>a</sup>	Load factor of BECCS plant <sup>b</sup>	Daily electricity production	Data illustrated in
Dynamic simulation of different cases using the solar radiation and electricity demand data for July					
Case A	LF <sub>min</sub> = 0, α <sub>support</sub> = 0%	27.6%	72%	758.0 MWh	Fig. 7(a)
Case B	LF <sub>min</sub> = 21%, α <sub>support</sub> = 0%	27.4%	72%	758.0 MWh	Fig. 7(b)
Case C	LF <sub>min</sub> = 21%, α <sub>support</sub> = 30%	26.1%	56%	651.3 MWh	Fig. 7(c)
Case D	LF <sub>min</sub> = 21%, α <sub>support</sub> = 60%	24.1%	37%	529.6 MWh	Fig. 7(d)
Dynamic simulation of case C (LF <sub>min</sub> = 21%, α <sub>support</sub> = 30%) for various months					
January	LF <sub>min</sub> = 21%, α <sub>support</sub> = 30%	26.0%	28%	331.4 MWh	Fig. 9(a)
April	LF <sub>min</sub> = 21%, α <sub>support</sub> = 30%	25.3%	34%	396.8 MWh	Fig. 9(b)
July	LF <sub>min</sub> = 21%, α <sub>support</sub> = 30%	26.1%	56%	651.3 MWh	Fig. 9(c)
October	LF <sub>min</sub> = 21%, α <sub>support</sub> = 30%	26.0%	31%	362.4 MWh	Fig. 9(d)
Year (average)	–	26.6%	41%	469.0 MWh	–

<sup>a</sup> The net plant efficiency was calculated using Eq. (4) for every hour of the day, and the reported value is the electricity output-weighted average of the hourly efficiencies; <sup>b</sup> the average load factor of the BECCS plant was calculated by dividing the actual daily thermal output of the BECCS plant by the theoretical maximum thermal output (58.7 MW × 24 h)

### 3.3 The storage requirements for O<sub>2</sub>+CO<sub>2</sub> and CO<sub>2</sub>

The results from the dynamic simulation for the year allow to calculate the gas storage requirements. The storage requirements for O<sub>2</sub>+CO<sub>2</sub>, which is used for oxy-fuel combustion, are calculated in this section. Simultaneously, a similar amount of recycled CO<sub>2</sub> has to be stored for utilisation in the CLAS process (not calculated here). The highest storage requirement for O<sub>2</sub>+CO<sub>2</sub> is in the summer (i.e. July), when up to 779 t of the gas has to be stored for later use (working gas). Assuming additional 500 t of O<sub>2</sub>+CO<sub>2</sub> as a buffer gas, the storage has to accommodate 1279 t of O<sub>2</sub>+CO<sub>2</sub>. In January, the O<sub>2</sub>+CO<sub>2</sub> storage requirement is the lowest: only 876 t (500 t buffer gas + 376 t working gas) has to be stored, as a lower solar power input results in a lower O<sub>2</sub> production. The hourly amount of storage for the different seasons is illustrated in Fig. 10, below.

The volume required for storage in July corresponds to 215,066 m<sup>3</sup>, which is comprised of 130,990 m<sup>3</sup> for working gas and 84,076 m<sup>3</sup> for buffer gas. This calculation assumes a density of the O<sub>2</sub>+CO<sub>2</sub> mixture (27.0 vol% O<sub>2</sub>+CO<sub>2</sub>) of 5.947 kg/m<sup>3</sup> at 20 °C and 6 bar. In comparison, the average working gas capacity of the salt caverns in Europe that were in operation as of end 2016 is 389,362 m<sup>3</sup>, which is almost two times the volume required for the process of this study (Cornot-Gandolphe 2017). We assumed operation of the cavern in the pressure range between 2 and 6 bar—higher pressures would increase inefficiencies during compression and de-compression. However, caverns with a smaller volume could be used with a higher operating pressure to meet the gas storage requirements, or alternatively (additional) surface gas storage could be erected.

### 3.4 Factors effecting the efficiency of the process

The net plant efficiency is significantly impacted by the thermal efficiency of the steam cycle. The latter is 43.7%. During sole operation of the CSP-CLAS plant (i.e. at mid-day), the thermal efficiency of the system is 17.8% (assuming a solar field efficiency, η<sub>HS+R</sub>, of 49.0%). This is slightly lower than a CSP plant with the same solar field (49.0%) and steam cycle efficiency (43.7%) in which the incoming solar power at the receiver is directly

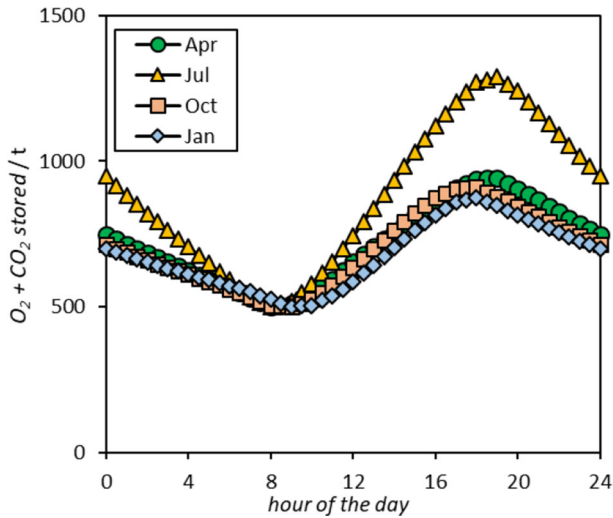


**Fig. 10** The change of mass of  $O_2+CO_2$  (27 vol%  $O_2+CO_2$ ) stored over the course of the day for different months

transferred to the steam cycle (21.4%) (Zhang et al. 2013). A minor part of this energy penalty can be attributed to some heat being lost (1.1%), e.g. when discharging the  $O_2$ -deficient air at 70 °C to the atmosphere or when storing the  $O_2+CO_2$  with 80 °C in the underground. Though, the major part of the energy penalty comes from the steam requirements for loop-seal fluidisation, which is withdrawn from the inlet of the low-pressure turbine. The reduction in electricity production varies depending on the oxygen carriers' support loading in the range between 12.2% (unsupported) and 15.1% (60 wt%  $Al_2O_3$ ). It is worth mentioning that in the CLAS process, the steam requirements for loop-seal fluidisation are typically larger than during the CLC process, owing to a lower  $O_2$  storage capacity of the active phases. For example, in the case of Mn-based oxygen carriers, the transition between  $Mn_2O_3$  and MnO during in a fuelled CLC process corresponds to an  $O_2$  storage capacity of 10.1 wt%, while the transition between  $Mn_2O_3$  and  $Mn_3O_4$  results in an  $O_2$  storage capacity of only 3.4 wt%. To provide the same amount of  $O_2$  per unit of time, the oxygen carrier circulation rate has to be three times higher in the CLAS process than in the CLC process assuming full conversion. When assuming the steam requirements scale linearly with the oxygen carrier circulation rate, three times more steam is required for the fluidisation of the loop-seals. The thermal efficiency of the process during sole operation of the BECCS plant is 37.0%; this efficiency could be increased by operation of the oxy-fuel combustor at elevated pressure and expansion of the combustion products using a gas-turbine for additional electricity generation (i.e. a combined cycle approach). However, since the remaining parts of the process were already relatively complex, it was decided not to increase the complexity further.

### 3.5 The $CO_2$ capture rate of the system

Using the results of the dynamic simulation, the amount of  $CO_2$  captured was calculated. A capture efficiency of 98% was assumed. The hourly results for the different months are shown in Fig. 11, below.

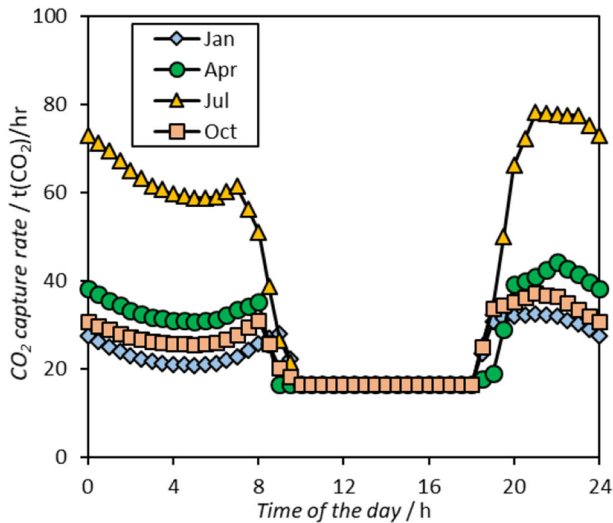


**Fig. 11** The hourly CO<sub>2</sub> capture rate of the system simulated for different months. The oxygen carriers were Mn<sub>2</sub>O<sub>3</sub> supported on 30 wt% Al<sub>2</sub>O<sub>3</sub> and a minimum load factor of 21% for the BECCS plant was assumed

Figure 11 shows that the daily amounts of CO<sub>2</sub> captured vary seasonally between January (543.1 t/day) and July (1067.5 t/day). Over the course of a year, the process is able to capture 260,517 tonnes of CO<sub>2</sub>.

## 4 Conclusions

We report the results of a dynamic simulation of a system that combines a CSP-CLAS process with an oxy-fuel combustion process for CO<sub>2</sub> capture. The fuel for the combustion is olive tree pruning, which is a locally produced agricultural residue. The CSP process was sized for a maximum concentrated solar power heat flow of 100 MW into the reducer (i.e. reached at mid-day in the summer months). It was calculated that the system is able to utilise 2.43% of Andalusia's olive tree pruning production, thereby capturing 260.5 k-tonnes of CO<sub>2</sub> per year and producing an average power output of 18 MW. Owing to the synergies of the two subprocesses, solar energy is effectively stored as O<sub>2</sub>+CO<sub>2</sub> during the day, which allows for operation of the BECCS process for the production of negative CO<sub>2</sub> emissions predominantly at night. When using the solar beam irradiance data for July and using ideal assumptions (unsupported Mn<sub>2</sub>O<sub>3</sub> oxygen carriers and no minimum load factor for the BECCS plant), it was possible to achieve an electricity output that is proportional to Spain's electricity demand, thereby constantly providing 0.10% of Spain's electricity. However, when supporting the active metal oxide and setting a minimum load factor of the BECCS plant of 21%, the O<sub>2</sub> production and thus the solar energy storage potential decreased significantly. This resulted in the production of excess energy at mid-day. Furthermore, it was found that when considering steam requirements for loop-seal fluidisation (the steam was taken from the inlet of the low-pressure turbine), the electricity production from the enthalpy transferred from the CLAS process to the steam cycle decreased by 12.2–15.1% for oxygen carrier support loadings of 0–60 wt%. This study also showed that dynamic simulations over the course of a year are essential to predict the performance of such synergetic processes realistically: In colder



months, with less available solar power, the process provides a significantly lower electricity output. For example, the average daily electricity production in January is 331.4 MWh, while the value for July is 631.2 MWh. Furthermore, relatively large gas storages are required, which either decrease the number of possible locations (e.g. has to be situated near a salt cavern that is suitable for gas storage) or expensive surface gas tanks have to be constructed.

Despite several drawbacks and the relatively high complexity of this process, it might still be a promising negative emissions technology (NET). It shall be remembered that the main objective of the process of this study is not the production of inexpensive electricity, but an economically viable net removal of CO<sub>2</sub> from the atmosphere. The cost of CO<sub>2</sub> capture (subsidised by the selling of electricity) will likely be lower than that of first-generation direct air capture systems, and the economics of the process will further improve when considering a (future) price on CO<sub>2</sub> emissions (e.g. carbon tax). Furthermore, the process utilises a locally produced agricultural residue, which is favourable as it eliminates the risk that the production of the fuel (biomass) is competing with the production of food, and excessive CO<sub>2</sub> emissions for the transport of the fuel are unlikely.

To ultimately assess the performance and economics of this process, further in-depth studies are needed that focus on specific design aspects (e.g. improvement of loop-seals), operational aspects (e.g. effect of short-term fluctuations in solar radiation on the reactor temperature and thus O<sub>2</sub> production rate, the effect of the support material on the oxygen carrier lifetime), economic aspects (e.g. a detailed calculation of the capital and operating costs of the process) and environmental aspects (e.g. the compilation of a life cycle assessment).

#### 4.1 Strategy recommendations

Though the process studied in this work is relatively complex (e.g. when considering the number of reactors) and its thermal efficiency is inferior to state-of-the-art fossil fuel power plants, it is still promising. This is because it utilises a waste product (agricultural residues), which is inexpensive and abundant, thereby enabling the net removal of CO<sub>2</sub> from the atmosphere. It was calculated that the system in this study sequesters the carbon from 2.43% of Andalusia's annual olive grove (*Olea europaea*) production. Thus, 41 of such systems (or other BECCS systems with a similar fuel burn rate) could utilise Andalusia's entire olive grove production, thereby capturing 10.72 million tons of CO<sub>2</sub> annually. Figure 2 shows that other types of biomass are readily available in Andalusia for use in BECCS processes. Other parts of the world also produce annually high quantities of agricultural residues (e.g. shell, straw and stalk of agricultural plants), such as root crops (e.g. *Dioscorea alata*) in Africa (55.0 million tonnes); wheat (*Triticum*) and rice (*Oryza sativa*) in Asia (835.6 million tonnes); sugar cane (*Saccharum officinarum*), maize (*Zea mays*) and legumes (*Fabaceae*) in Latin America (157.6 million tonnes); and wheat (*Triticum*) in Europe, the former Soviet Union and Oceania (291.3 million tonnes) according to Hall et al. (Hall and Overend 1987). When considering all types of agricultural crops, the total mass of agricultural residues annually produced worldwide was estimated to be 3135 million tonnes (Hall and Overend 1987). A more recent calculation by Lal (2005)—though not divided by region—was based on the data of the Food and Agriculture Organization of the United Nations (FAO 2002). It estimated the annual global agricultural residue production to be 3758 million tonnes. Given the large quantity of residues and waste being produced worldwide, many of such niche processes with inherent CO<sub>2</sub> capture, tailored to location and fuel's characteristics, could play a crucial role in the reduction of global CO<sub>2</sub> emissions. We recommend that new processes that

utilise waste products and residues for CO<sub>2</sub>-neutral or CO<sub>2</sub>-negative electricity generation should be screened for economic viability under consideration of a (future) carbon tax, integration potential with a likely electricity grid system, and using the local conditions and real data. As done in this work, the combination of energy systems using different types of energy carriers (here solar and biomass) should be tested in combination to identify synergies. Instead of curtailing excess solar and wind power, it should be used (when reasonable) for power storage, conversion and production.

**Funding information** This work was funded by the Engineering and Physical Sciences Research Council (EPSRC) as part of the RCUK Energy Programme under EP/P026214/1. The authors thank the Department of Chemical Engineering at Imperial College London and the Public Authority of Applied Education and Training in Kuwait for the funding of PhD scholarships.

**Open Access** This article is distributed under the terms of the Creative Commons Attribution 4.0 International License (<http://creativecommons.org/licenses/by/4.0/>), which permits unrestricted use, distribution, and reproduction in any medium, provided you give appropriate credit to the original author(s) and the source, provide a link to the Creative Commons license, and indicate if changes were made.

## References

- AspenTech (2013) ASPEN Plus - Getting Started Modeling Processes with Solids. Version Number: V8.4. Aspen Technology, Inc., Burlington
- Barlev D, Vidu R, Stroeve P (2011) Innovation in concentrated solar power. *Sol Energy Mater Sol Cells* 95(10): 2703–2725
- Blair N, DiOrio N, Freeman J, Gilman P, Janzou S, Neises T and Wagner M (2018) System Advisor Model (SAM). [www.nrel.gov/docs/fy18osti/70414.pdf](http://www.nrel.gov/docs/fy18osti/70414.pdf). Accessed 31 March 2019
- Cho P, Mattisson T, Lyngfelt A (2004) Comparison of iron-, nickel-, copper- and manganese-based oxygen carriers for chemical-looping combustion. *Fuel* 83(9):1215–1225
- Cornot-Gandolphe S (2017) Underground Gas Storage in the World - 2017 Status. Cedigaz Insights No. 22
- ENTSOE (2018) The European Network of Transmission System Operators for Electricity: hourly load values of a specific country: Spain. [www.entsoe.eu](http://www.entsoe.eu). Accessed 28 December 2017
- FAO (2002) FAO Production Yearbook 2001. Statistics Div., Food and Agricultural Organization of the United Nations (FAO), Rome
- García-Maraver A, Zamorano M, Ramos-Ridao A, Díaz LF (2012) Analysis of olive grove residual biomass potential for electric and thermal energy generation in Andalusia (Spain). *Renew Sust Energy Rev* 16(1):745–751
- Hall DO, Overend RP (1987) Biomass: Regenerable Energy (World Energy Options). Wiley-Blackwell
- IPCC (2005) IPCC special report on carbon dioxide capture and storage. Cambridge University Press, Cambridge
- Karlsson H, Byström L (2011) Global status of BECCS projects 2010. Australia, Global CCS Institute, Canberra
- Lal R (2005) World crop residues production and implications of its use as a biofuel. *Environ Int* 31(4):575–584
- Li Z-s, Zhang T, N-s C (2008) Experimental study of O<sub>2</sub>-CO<sub>2</sub> production for the oxyfuel combustion using a CO-based oxygen carrier. *Ind Eng Chem Res* 47(19):7147–7153
- Lyngfelt A, Leckner B, Mattisson T (2001) A fluidized-bed combustion process with inherent CO<sub>2</sub> separation; application of chemical-looping combustion. *Chem Eng Sci* 56(10):3101–3113
- Marx K, Bertsch O, Pröll T, Hofbauer H (2013) Next scale chemical looping combustion: process integration and part load investigations for a 10MW demonstration unit. *Energy Procedia* 37:635–644
- Moghtaderi B (2010) Application of chemical looping concept for air separation at high temperatures. *Energy Fuel* 24(1):190–198
- NREL (2018) Concentrating solar power projects: Planta Solar 10. [https://www.nrel.gov/csp/solarpaces/project\\_detail.cfm/projectID=38](https://www.nrel.gov/csp/solarpaces/project_detail.cfm/projectID=38). Accessed 28 December 2017
- Porrizzo R, White G, Ocone R (2016) Techno-economic investigation of a chemical looping combustion based power plant. *Faraday Discuss Chem Soc* 192:437–457
- Riaza J, Gil MV, Álvarez L, Pevida C, Pis JJ, Rubiera F (2012) Oxy-fuel combustion of coal and biomass blends. *Energy* 41(1):429–435

- Shah K, Moghtaderi B, Wall T (2012) Selection of suitable oxygen carriers for chemical looping air separation: a thermodynamic approach. *Energy Fuel* 26(4):2038–2045
- Shah K, Moghtaderi B, Wall T (2013) Effect of flue gas impurities on the performance of a chemical looping based air separation process for oxy-fuel combustion. *Fuel* 103:932–942
- Song H, Shah K, Doroodchi E, Wall T, Moghtaderi B (2014) Analysis on chemical reaction kinetics of CuO/SiO<sub>2</sub> oxygen carriers for chemical looping air separation. *Energy Fuel* 28(1):173–182
- Tagliaferri C, Görke R, Scott S, Dennis J, Lettieri P (2018) Life cycle assessment of optimised chemical looping air separation systems for electricity production. *Chem Eng Res Des* 131:686–698
- Vamvuka D, Tsamourgeli V, Galetakis M (2014) Study on catalytic combustion of biomass mixtures with poor coals. *Combust Sci Technol* 186(1):68–82
- Zerobin F, Bertsch O, Penthor S, Pröll T (2016) Concept study for competitive power generation from chemical looping combustion of natural gas. *Energy Technol* 4(10):1299–1304
- Zhang HL, Baeyens J, Degreè J, Cacères G (2013) Concentrated solar power plants: review and design methodology. *Renew Sust Energ Rev* 22:466–481
- Zhou C, Shah K, Moghtaderi B (2015) Techno-economic assessment of integrated chemical looping air separation for oxy-fuel combustion: an Australian case study. *Energy Fuel* 29(4):2074–2088

**Publisher's note** Springer Nature remains neutral with regard to jurisdictional claims in published maps and institutional affiliations.